

Review

Advances Using Single-Particle Trajectories to Reconstruct Chromatin Organization and Dynamics

O. Shukron,^{1,5} A. Seeber,^{2,5} A. Amitai,^{3,4,5} and D. Holcman ^{1,*}

Chromatin organization remains complex and far from understood. In this article, we review recent statistical methods of extracting biophysical parameters from *in vivo* single-particle trajectories of loci to reconstruct chromatin reorganization in response to cellular stress such as DNA damage. We look at methods for analyzing both single locus and multiple loci tracked simultaneously and explain how to quantify and describe chromatin motion using a combination of extractable parameters. These parameters can be converted into information about chromatin dynamics and function. Furthermore, we discuss how the timescale of recurrent encounter between loci can be extracted and interpreted. We also discuss the effect of sampling rate on the estimated parameters. Finally, we review a polymer method to reconstruct chromatin structure using crosslinkers between chromatin sites. We list and refer to some software packages that are now publicly available to simulate polymer motion. To conclude, chromatin organization and dynamics can be reconstructed from locus trajectories and predicted based on polymer models.

Exploring Chromatin Mobility

Fundamental physical properties of DNA, such as its internal elasticity, bending properties, and rotational energy, have been estimated *ex vivo* [1,2]. But what about the properties of chromatin *in vivo*? Not only has it been difficult to visualize specific chromatin loci, but it remains unclear what physical properties should be measured. Shall we simply use classical physical **observables** (see [Glossary](#)) or shall we focus on extracting other latent parameters? The choice of what to measure is open to bias. In the case of chromatin, we still do not have a complete and definitive physical model that would recapitulate and explain its dynamics and structure. However, recent works have advanced chromatin models to the point that they can predict changes in organization and dynamics [3,4]. Here, we review work combining **single-particle trajectories (SPTs)** of chromatin loci with **polymer modeling**. The aim of this review article is to clarify how experimental observation of chromatin dynamics can be related to its underlying structure using those models. As an example, we focus our attention on the chromatin response to DNA damage. While this review focuses also on connecting chromatin dynamics and with polymer models, others have reviewed different aspects of chromatin mobility (see [5–8]).

Early on, it was recognized that DNA is compacted into chromatin. Because this structure coils back on itself and has a repeating unit (see early studies showing chromatin as beads on a string), it was natural to start describing it as a polymer. Taking a coarse-grained approach, one could use a polymer model where the beads are connected by springs, repulse one another (**Lennard-Jones forces**), and have bending elasticity as a starting point for modeling chromatin (reviewed in [9]) (Box 1). Building on such a model and accounting for new experimental results

Highlights

Chromatin organization and dynamics can be reconstructed from loci trajectories. Biophysical parameters are often extracted from single chromatin loci single-particle trajectories (SPTs).

Statistical methods are being used to study the dynamics of multiple chromatin loci.

Chromatin properties can be described by polymer models.

Available packages exist for coarse-graining chromatin reconstruction.

¹Group of Data Modeling, Computational Biology and Predictive Medicine, Institut de Biologie, CNRS/INSERM/PSL Ecole Normale Supérieure, Paris, 75005, France
²Center for Advanced Imaging, Northwest Building, 52 Oxford St, Suite 147, Harvard University, Cambridge, MA, 02138, USA

³Department of Chemical Engineering, Institute for Medical Engineering and Science, Massachusetts Institute of Technology, Cambridge, MA, USA

⁴The Ragon Institute of MGH, MIT, and Harvard, Cambridge, MA

⁵These authors contributed equally to this work

*Corresponding author.
david.holcman@ens.fr (D. Holcman).



Box 1. Modeling Chromatin with Polymer Model

How do we model chromatin? Polymer modeling is a powerful tool, but finding the appropriate polymer model remains challenging and often depends on the scale and the question to be answered. The simplest model, which has already provided much insight into chromatin dynamics in a free and confined environment, is the Rouse model, that consists of beads connected by harmonic springs. The potential energy is

$$\phi_{Rouse} = (R_1, \dots, R_N) = \frac{\kappa}{2} \sum_{n=1}^N (R_n - R_{n-1})^2, \quad [i]$$

where the spring constant $\kappa = 3k_B T/b^2$ is related to the standard deviation b of the distance between adjacent monomers [81], with k_B the Boltzmann coefficient and T the temperature. The dynamics of monomer R_n is

$$\frac{dR_n}{dt} = -D \nabla_{R_n} \phi_{Rouse} + \sqrt{2D} \frac{d\omega}{dt}, \quad [ii]$$

for $n = 1, \dots, N$ and ω_n are independent 3D white noise with mean 0 and variance 1. It is possible to add the Lennard Jones (LJ) potential. To account for the LJ forces, we use the potential energy defined by

$$U(R_1, \dots, R_N) = U_{spring}(R_1, \dots, R_N) + U_{LJ}(R_1, \dots, R_N), \quad [iii]$$

where the spring potential is

$$U_{spring}(R_1, \dots, R_N) = \frac{\kappa}{2} \sum_{i=1}^{N-1} (|r_{i,i+1} - l_0|)^2, \quad [iv]$$

where l_0 is the equilibrium length of the bond. When we write $\kappa = \frac{3}{s_0^2}$ then s_0 is the standard deviation of the bond length (e.g., $s_0 = 0.2l_0$). Note that $U_{LJ}^i(r_{i,j})$, with $r_{i,j} = R_i - R_j$ and

$$U_{LJ}^i(r_{i,j}) = \begin{cases} 4 \left[\left(\frac{\sigma}{r_{i,j}} \right)^{12} - 2 \left(\frac{\sigma}{r_{i,j}} \right)^6 + \frac{1}{4} \right], & \text{for } |r_{i,j}| \geq 2^{1/6} \sigma \\ 0, & \text{for } |r_{i,j}| < 2^{1/6} \sigma, \end{cases} \quad [v]$$

where σ is the distance at which the potential is negligible. This distance remains to be found. With the choice $l_0 = 2\sigma$, the springs that materialize bonds cannot cross each other in stochastic simulations.

We briefly summarize the construction of a randomly crosslinked (RCL) polymer [14]: it consists of a linear backbone of monomers connected by springs, with an additional N_c added connectors between randomly chosen non-nearest neighbor monomer pairs. The energy of the RCL is the sum of two contributions, one from the backbone (Rouse) plus a contribution from the random connectors:

$$U(R_1, \dots, R_N) = \frac{\kappa}{2} (U_{Rouse} + U_{random}^{\mathcal{G}}), \quad [vi]$$

where $U_{random}^{\mathcal{G}} = \sum_{m,n} (R_m - R_n)^2$, is the potential energy from N_c added spring connectors (realization \mathcal{G}), and the sum extends to pairs (m,n) such that $|m - n| > 1$ (i.e., R_m and R_n are not immediate neighbors along the linear backbone). A realization \mathcal{G} means that we chose randomly N_c monomer pairs to connect (see [14] for a description of physical properties).

The encounter probability between monomers, which depends on the number of added connectors N_c , is usually a free parameter to be fitted from empirical data. Using the RCL model, it is possible to fit the empirical loci encounter probability from HiC data and derive the minimal number of crosslinks in a genomic section at a coarse-grained resolution. The RCL model could therefore be used to obtain structural parameters, not necessarily contained in the HiC data, such as the radius of gyration, the MSD of any loci, and the mean first encounter time between any two loci.

Finally, we summarize the procedure of construction of a polymer model:

- (i) First, select the resolution to coarse-grain chromatin, so that one bead represents a given X kbps. For example, $X = 3$ kbps with 100 beads, leads to a representation of 3 Mbp.
- (ii) Add connectors if necessary (see RCL description above) to represent chromatin compaction having a similar encounter probability matrix as the one obtained from HiC data. This procedure is nontrivial and described in [14].
- (iii) Generate numerical simulations of the polymer. Make sure to simulate enough time to reach steady-state.
- (iv) Collect enough realizations (Box 2) and apply the statistical estimators for evaluating quantities of interest.
- (v) Special care should be given to the case of transient simulations, such as the consequences of a DSB. Set time $t = 0$ exactly when connectors are removed post-DSB. In that case, the polymer is locally out of equilibrium. Removing local forces or tethering forces at the initial time can lead to chromatin reorganization at short- and long-scale [80] timescale.

Glossary

Anomalous diffusion: stochastic processes, the statistics of which deviates from that of a classical Brownian motion. It is characterized by an MSD with a nonlinear relationship with time. When $\alpha > 1$, the locus motion is described as superdiffusive (the motion contains a drift component), while for $\alpha < 1$ the motion is called subdiffusive (constrained by obstacles or tethering forces).

β -Polymer model: a polymer model with long-range interactions between monomers, that can be modulated so that the anomalous exponent α of any internal monomer is prescribed to a given value α in the range (0–0.5).

Brownian motion: mathematical limit of a random walk when the time steps Δt tends to zero (construction of Paul Levy).

Cohesin: a protein complex that holds replicated sister chromatids together after DNA replication. It is involved in DSB repair. This complex has a role in chromatin organization in G1 phase of the cell cycle. Cohesin removal from DNA increases chromatin dynamics.

Confined motion: result of a motion restricted by impenetrable obstacles or by a field of force.

CTCF: CCTC-binding factor containing 11 zinc finger binding domains. It is involved in 3D chromatin organization by loop formation, as anchor points and in boundary formation.

Diffusion: collective motion of Brownian particles. The probability density function or the concentration (number of particle per unit of volume) satisfies the diffusion equation.

Double-strand break (DSB): this is a type of DNA damage where both strands of DNA are cleaved.

Effective spring coefficient (K_c): a spring force applied to a monomer of a polymer results in a tether or anchor. Used to infer the resulting tethering interactions around a chromatin locus.

HiC data: a certain type of chromosomal capture data, providing the histogram of encounters between any two genomic loci resulting from physical proximity or DNA-protein cross-linking.

Homologous recombination (HR): also called homology directed repair, this DNA double-strand break repair pathway relies on using a donor template to repair the damage site.

coming from **HiC**, long-range interactions between distant chromatin sites have been addressed in simulations [10–12] and theory [13,14]. Although these models are used to simulate chromatin in some defined conditions, how they relate to the biological analog remains unclear.

To determine polymer models that infer the actual behavior of chromatin inside the nucleus, one must be able to compare extracted physical parameters from real experimental chromatin data with those predicted from the model. To this end, the adoption of fluorophores, such as green fluorescent protein, combined with bacterial operator array systems to visualize single chromosomal loci live and *in vivo*, created the subfield of chromatin dynamics [15]. More recent developments using dCas9 and modified guide RNAs, as well as new bacterial arrays, have expanded the live cell imaging chromatin toolbox, reviewed in [16,17]. These tools have advanced our knowledge of what regulates chromatin movement. In particular, research in budding yeast, performed by many laboratories over two decades, has elucidated a partial framework of the regulators of chromatin movement. While the important fine details are better reviewed elsewhere [16], we highlight a few key regulators.

To start, chromatin motion depends on intracellular ATP levels. Glucose starvation or treatment of cells with either sodium azide or the mitochondrial uncoupler carbonyl cyanide *m*-chlorophenylhydrazine (CCCP), all of which deplete ATP, reduce chromatin motion [18–23]. In addition to ATP, the cell cycle stage has a dramatic effect on chromatin movement where chromatin moves less in S phase and is much more dynamic in G1 phase. This effect is conserved from yeast to human cells [18,24–26]. The effect depends on DNA replication and artificial cleavage of **cohesin** in S phase restores mobility to G1 levels [27]. Chromosome tethers also play a role in restricting chromatin movement. A clear example is the Rab1 configuration of chromosomes in budding yeast, whereby the telomeres transiently associate with the nuclear periphery and the centromeres are attached to the spindle pole body [28,29]. These attachments restrict motion and when artificially removed increase chromatin dynamics. Although yeast do not have a nuclear lamina, the loss of chromosome tethering by ablation of lamin A in mammalian cells leads to increased chromosome dynamics [19,30–34]. Another master regulator of chromatin movement is nucleosome occupancy. Work on the chromatin remodeling enzyme, **INO80**, showed that direct targeting of INO80 to a chromosomal locus was sufficient to increase the dynamics of that locus [35]. Loss of nucleosomes on DNA through other means, either by the depletion of Nhp6, the budding yeast version of high mobility group protein B1 (HMGB1), or the transcriptional downregulation of histone genes, also increases global chromatin dynamics [3]. Thus, many regulators of chromatin dynamics have been described. What is still little understood is the function of chromatin movement.

While chromatin mobility can be regulated experimentally, proving that it has a role in cellular processes has been difficult. An early postulated role for mobility was transcription. This was supported by evidence that artificial activation of transcription by targeting the viral transactivator protein VP16 to a transgene array in mammalian cells causes the locus to undergo directional movement away from the nuclear periphery [36]. Consistently, targeting of VP16 to a yeast telomeric locus also drives this locus away from the periphery and VP16 targeting to a locus on the middle of a chromosomal arm increases its dynamics [35]. However, targeting of another transcriptional activator, Gal4, did not increase locus dynamics nor did the inhibition of transcription in yeast cells [35]. The effect of transcription in higher eukaryotes, in general, is less clear and has been correlated with decreased motion [37]. Others have shown that inhibition of RNA polymerase II increases chromatin motion and that transcription may serve to stabilize networks of chromatin domains [38–40]. Measuring chromatin movement during enhancer and promoter contact still remains relatively unstudied. Another role in which chromatin movement may serve

INO80: this protein complex is involved in nucleosome remodeling at the site of DNA DSBs. It consists of many proteins, including the catalytic Ino80 and the actin-related proteins, Arp5 and Arp8. Artificial targeting of this protein to a chromatin locus increases its dynamics in yeast.

Length of constraint (L_c): the standard deviation of locus position with respect to its mean averaged over time. Estimates the space explored by a locus trajectory.

Lennard-Jones force: a physical force that models short-range repulsion and long-range attraction between two monomers using a potential well. It is used to prevent a polymer chain from collapsing to a point at equilibrium.

Mean square displacement (MSD): second moment of a stochastic process $X(t)$ computed as $\langle (X(t + \Delta t) - X(t))^2 \rangle \approx A\Delta t^\alpha$ (for Δt small). It is computed by averaging over trajectory realization. When $X(t) = x$, the MSD is computed at point x . When there are not enough trajectories, the MSD is often approximated by its value along a single trajectory that could create a bias in the statistics, especially when the medium is not homogeneous.

Observables: physical quantities that can be measured.

Passage time analysis: analysis of the statistics associated with continuous random processes crossing a threshold. Examples are the escape from potential well (activation escape), escape through a small hole (narrow escape), or polymer looping (time for the two extremities to enter into a ball of small radius ϵ).

Polymer modeling: mathematical idealization of a continuum polymer chain, approximated by point (bead) connected by springs. More forces can be added, such as bending elasticity, torsion forces, and many more. A polymer model is an avatar of chromatin inside a computer.

Random walk: sequences of points, where the increment between two consecutive points is obtained from a Gaussian distribution with a fixed time step Δt .

Randomly crosslinked (RCL) model: polymer model where monomer pairs are connected randomly. The RCL model is used to infer the minimum number of permanent crosslinks in chromatin region from chromosome conformation capture data.

Rouse polymer model: the most elementary polymer model whereby

is the efficiency of repair of **DNA double-strand breaks (DSBs)** by a process called **homologous recombination (HR)**, discussed in [3]. Here, a broken DNA strand must physically scan the nucleus to find its homologous partner if the replicated sister is not present or is otherwise damaged. While definitive proof that chromatin motion facilitates repair by HR remains elusive, there are a number of correlations. In budding yeast, induction of a DSB and activation of the DNA damage checkpoint, a control mechanism in the cell-division cycle that ensures that mitosis does not occur until damaged DNA has been repaired, increases chromatin motion both locally and globally [41,42]. Ablation of proteins that result in reduced movement decreases repair efficiency by HR [41], while mutations that increase movement improve HR efficiency [3,35]. Ultimately, these still remain correlations and an experiment directly showing that enhanced movement increases repair by HR is still lacking.

In general, chromatin movement has been studied by analyzing single locus trajectories and plotting the **mean square displacement (MSD)**. From this, a radius of constraint or volume of space explored by the locus can be extracted. A number of recent studies have published methods on extracting hidden directed motion within trajectories using methods such as directional change distribution analysis or computational methods to identify long-lasting directed motions [43,44]. In addition to these useful tools, we and others have asked the question, ‘what other information can be obtained from trajectories?’. The goal of this review is to present advances in single-particle trajectory analysis and to illustrate how extracted parameters can be used in polymer models to make biological predictions.

This review is organized as follows. We first describe **diffusion** models that have been used to analyze chromatin trajectories. We introduce four key physical parameters that can be extracted from chromatin loci trajectories and can be used in combination to characterize motion. We then focus on the selection of polymer models and describe how the sampling time step influences the extracted statistical observables from the trajectories. Next, we will present how to perform a correlation analysis for two loci recorded simultaneously and we will discuss physical constraints on chromatin and describe an approach to estimate the number of crosslinkers between chromatin loci. Finally, we summarize publicly available software packages for polymer simulations (see the supplemental information online). Although many examples described here concern yeast, the statistical methods and data analysis can be applied to many other organisms, from insects to mammalian cells [37,45,46].

Chromatin Locus Dynamics Revealed by SPTs

SPTs consist of an ensemble of successive points acquired at a sampling rate Δt . What physical observables can be extracted from these trajectories? To answer this question a physical diffusion model (not to be confused with a polymer model) should be selected. The model chosen to fit an MSD curve must provide plausible physical mechanisms and accurate predictions. Examples of physical models include **Brownian motion** or **random walk** (which is a discretized version of a Brownian motion at a time step Δt) and **anomalous diffusion**. Selection of the correct model remains challenging because not all loci behave similarly. Failure to select the correct model will prevent accurate extraction of parameters. A recent study used a Bayesian inference approach to automate MSD model selection across trajectories throughout the nucleus [47]. Others have published approaches to test for the goodness-of-fit of model assumptions and estimated parameters [48,49]. In the following section, we will briefly describe some physical models and what physical observable should be measured.

The most well-known example of passive molecular dynamics is classical free diffusion described by Brown in 1827 and quantified statistically by Einstein in 1905. A particle driven by free diffusion

beads are connected by springs. A Rouse polymer has an anomalous exponent $\alpha = 0.5$. In numerical simulations, the chain is allowed to cross itself.

Single-particle trajectory (SPT): causal collection of points represented by a time series of a single tagged molecule moving through a medium. The sampling time is Δt . In the context of the genome, SPTs are traces of the motion trajectory of a chromatin locus acquired in two or three dimensions.

Zeocin: a radiomimetic drug that induces random DNA damages, including DSBs.

at scale Δt is characterized by random jumps that follow a Gaussian distribution with zero mean and variance $2D\Delta t$, where D is the diffusion coefficient. In this case, the physical observable to estimate is simply the diffusion coefficient D . However, the locus motion can be restricted due to obstacles or to some resulting tethering force, which is not accounted for in classical Brownian motion. In that case, the extent of the restricted region and the nature of the restriction (confinement versus tethering force) must be determined. Another model used to describe the motion of a locus is a deviation of classical Brownian motion, called anomalous diffusion. Here, the forces underlying the locus dynamics are correlated in time [50]. In this case, the correlation modifies the nature of the dynamics (see section 'Anomalous exponent α '). Another possibility is that the particle motion observed by SPTs result from a combination of deterministic (generated by a force) and Brownian motion. The motion could also result from alternating between a deterministic force and diffusion. The nature of the force should be identified as well as the switching rate, often approximated as Poissonian (characterized by a single exponential parameter).

To summarize, we need to select a physical model, making an informed decision based on trajectory data. When successful, the underlying model can be used to extract specific parameters that characterize chromatin motion.

Parameters that Describe Chromatin Motion

In this section, we describe four parameters computed from SPTs that are used to characterize chromatin motion. They provide independent, complementary information on first and second moment statistics.

Length of Constraint L_c to Characterize Confined Motion

How much space does a locus explore? The majority of studies up to this point have used the plateau of an MSD curve to estimate the radius of constraint. This number, coupled with the size of the nucleus, can be used to estimate the relative volume of space a locus will move through. However, not all MSD graphs plateau and thus a plateau-independent parameter is required. We and others have proposed using another parameter, such as the standard deviation of the locus position with respect to its mean average over time [4,33], which we term the **length of constraint** L_c (Box 2). This parameter, like the radius of constraint, can be used to estimate the degree of confinement of a locus. A small L_c compared with the radius of the nucleus is thus the signature of a highly **confined motion**, while a large L_c means that the locus motion is not restricted by any nuclear bodies or chromatin. In summary, the length of constraint (L_c) provides a measure of confinement, but it does not reveal the underlying mechanism of motion.

Anomalous Exponent α

Anomalous diffusion is a type of random motion characterized by an anomalous exponent α , which is classically extracted from the slope of the (MSD) $\langle |X(t + \Delta t) - X(t)|^2 \rangle$ that behaves like At^α for Δt small over the time (Box 2). When $\alpha = 1$ it reflects Brownian motion, $\alpha > 1$ is called superdiffusion, which may represent a dynamic containing an element of deterministic (ballistic) directed motion. Finally, $\alpha < 1$ is a subdiffusive motion, which could result from forces between monomers/chromatin sites (see below) and/or the visco-elastic properties of the nuclear plasm [4,13,51,52]. When Δt is in the range of 30 to 300 ms, we estimate α from the first six time points of an MSD. However, we point out that the initial slope of an MSD curve is calculated using all time points and thus longer trajectories will provide a more accurate approximation of α . One way to compute the MSD is by taking the ensemble-average, averaging the displacements of multiple particles. The alternative is a time-averaged MSD, which averages all the displacements made by a single trajectory over a given period. The majority of single particle data on chromosomal loci is done on time-averaged MSDs.

As mentioned above, directed motion is often hidden in the MSD analysis. In that case, extracting the anomalous exponent is not enough to account for the entire dynamics. In parallel, a drift analysis has to be performed in order to extract the spatial distribution of vector fields, [53–55] and directional changes [44,56]. The exponent α computed for a single locus remains difficult to interpret and in particular to connect with local chromatin organization. α reveals much of the nature of a locus that belongs to a polymer but clearly remain insufficient, alone, to recover all the properties of chromatin. In general, the exponent α for chromatin loci varies in the range 0.3–0.5, when no external forces are applied to the polymer model [4]. But in the presence of deterministic forces, generated, for example, by nuclear oscillation, actin, or microtubule networks, the range of α can increase to 0.5–2. To give a few examples, for a Δt larger than 5 s, α was estimated around 0.4 for the GAL loci in yeast [57] under glucose or galactose. Another study [58] found $\alpha = 0.75$ for the same locus when the yeast was grown under glucose and 0.64 for galactose. Possible reasons for the discrepancy between these values could be differences between yeast strain backgrounds, localization error, or nuclear motion. For telomeres of mammalian cells, $\alpha \approx 0.32$, when the time series analysis is performed in the interval $[10^{-2}; 1]$ s [59], which is consistent with other studies [60,23], reporting 0.39 for chromosomal loci in bacteria. In general, phenomenological models of anomalous dynamics such as fractional Brownian motion [60] have been used to interpret these observations. However, as we will see below, much could be learned by using a polymer model, which

Box 2. Estimating Parameters from SPT of Chromatin Locus

We describe here how the four parameters (effective diffusion coefficient D_c , anomalous exponent α , length of constraint L_c , and tethering constant k_c are estimated from SPTs. $X(t_1), \dots, X(t_n)$: the minimum number of points that we used is around 10, but in practice, we recommend to use at least 100 points.

- The easiest parameter to estimate is L_c , as it requires pre-computation of only the center of mass of the confined trajectory. The length L_c is defined as the standard deviation of the locus position with respect to its mean averaged over time, and given by $L_c \approx \sqrt{\frac{1}{N} \sum_{k=1}^N (X(k\Delta t) - \langle X \rangle)^2}$, for n large and does not require more specific estimation [33,61].
- There are several possibilities to extract the diffusion coefficient D_c . To compute the diffusion coefficient of the tagged monomer or locus X_c , we can use the following empirical estimator [61] $D_c \approx \frac{1}{2dN_p\Delta t} \sum_{k=1}^{N_p-1} (X_c((k+1)\Delta t) - X_c(k\Delta t))^2$, in dimension d (2 or 3). It can also be extracted for a Brownian motion by fitting the tangent to the MSD starting from the origin. If loci motion contains both a drift and a diffusion part, Δt should not be too large.
- To estimate the anomalous exponent α , we first compute the MSD: it is defined as the squared displacement with respect to the initial trajectory position, averaged over time for a given loci X_c : $\text{MSD}(t) = \langle (X_c(t) - X_c(0))^2 \rangle$. For short times, $\text{MSD}(t) \approx Ct^c$, where $C > 0$. To extract the coefficient α , from empirical trajectories, it is possible to directly use the function Ct^c in linear coordinates rather than in log scale (which drastically reduces fluctuations), as shown in Figure 1A,B. For an empirical trajectory, we average over the successive time points rather than realizations by using formula $\text{MSD}(q\Delta t) \approx \frac{1}{(N-q)\Delta t} \sum_{k=1}^{N-q} (r(q\Delta t) - r(q\Delta t + k\Delta t))^2$, where N is the total number of trajectory points (Figure 1A,B). Then, we fit the first seven points of the curve to a power law. The difficulty is to find the correct time interval to fit the curve. Short and long time scales should be discarded (see Figure 1). We show an example in Figure 2C in main text, computed from averaging over the realization of many simulated trajectories.
- Because the chromatin interacts locally with its environment, we estimated the average interaction between chromatin and its local environment by a harmonic well of strength k acting on a single monomer \mathbf{R}_c . The potential energy of the interaction is $U(\mathbf{R}_n) = \frac{1}{2}k(\mathbf{R}_n - \boldsymbol{\mu})^2$, where $\boldsymbol{\mu}$ is the fixed position of the interaction. The velocity of an observed monomer \mathbf{R}_c , averaged over many trajectories, is driven by this interacting force, following relation [4] $\lim_{\Delta t \rightarrow 0} E \left\{ \frac{\mathbf{R}_c(t + \Delta t) - \mathbf{R}_c(t)}{\Delta t} \middle| \mathbf{R}_c(t) = \mathbf{x} \right\} = -Dk_{cn}(\mathbf{x} - \boldsymbol{\mu})$, where $\mathbf{R}_c(t)$ is the position of locus c at time t , D is the diffusion coefficient, and $E\{\cdot | \mathbf{R}_c(t) = \mathbf{x}\}$ means averaging over trajectory realizations such that the condition $\mathbf{R}_c(t) = \mathbf{x}$ is satisfied. Relation (*) links the average velocity of the observed monomer c to the force applied at a distance $|c - n|$. For a Rouse polymer, with a potential well $U(\mathbf{R}_c)$, the effective spring coefficient is given by $k_{cn} = \frac{k\kappa}{\kappa + |c - n|k}$, where κ is the monomer–monomer spring coefficient. The empirical estimator for k_{cn} computed along the locus trajectories $\mathbf{R}_c(t)$ is

$$k_c \approx \frac{1}{2(N_p - 1)} \sum_{i=1}^2 \sum_{h=1}^{N_p - 1} \frac{R_c^i((h+1)\Delta t) - R_c^i(h\Delta t)}{D_c \Delta t (R_c^i(h\Delta t) - \langle R_c^i \rangle)}, \quad [1]$$

in practice, to avoid dividing by a small number, it is better to fit the slope of the curve as shown in Figure 11.

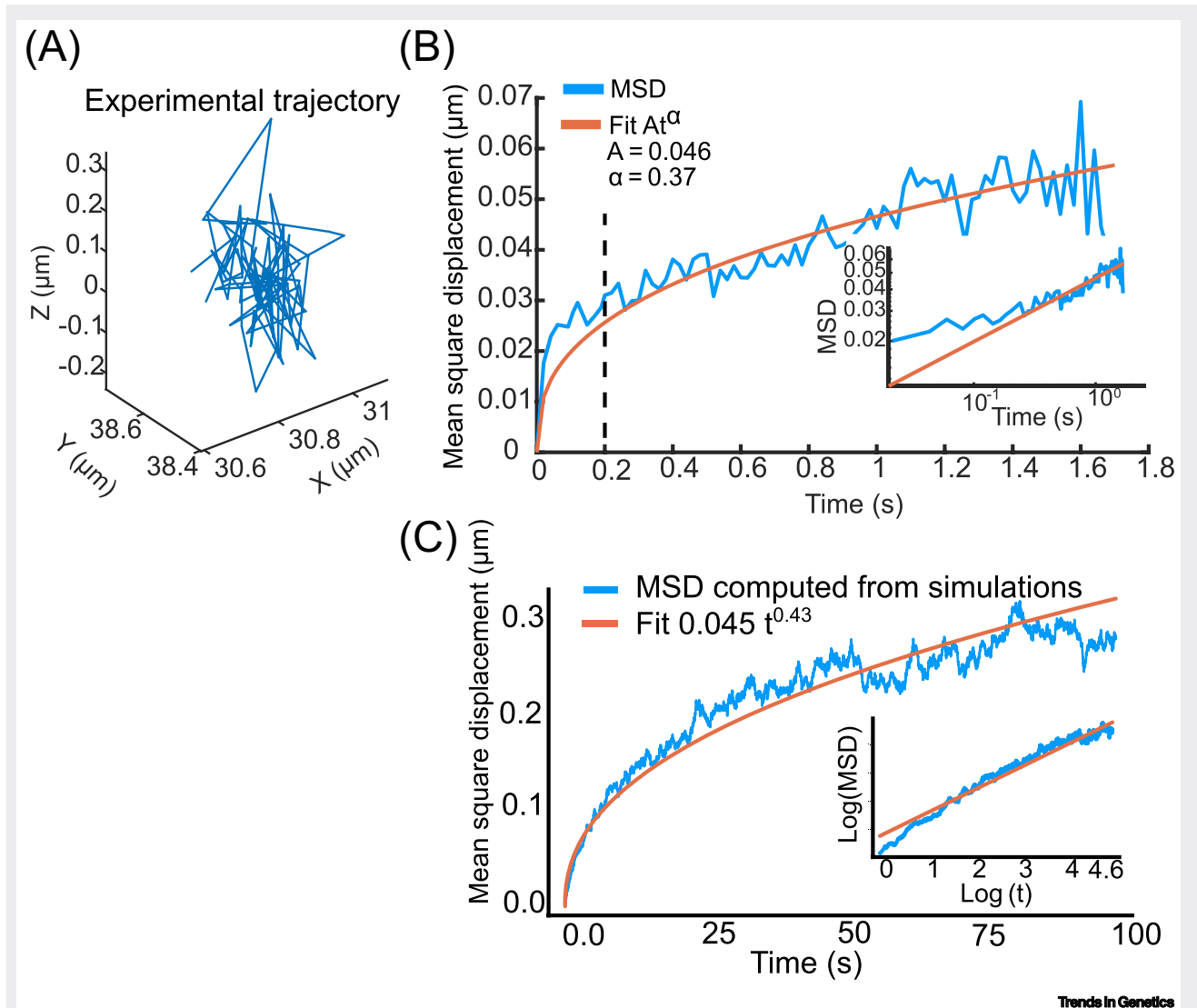


Figure 1. Plotting Mean Square Displacement (MSD) and Estimating the Anomalous Exponent α . (A) Sample empirical trajectory sampled at acquisition time of 20 ms up to 1.7 s. (B) MSD (blue), of the empirical trajectory in panel A, where we average over time lags instead of over trajectories, as performed in (C). We fit the MSD with the model At^α from 0.2 s to 1.7 s and obtain $A = 0.046$ and the anomalous exponent $\alpha = 0.37$. (C) The MSD curve (blue) is computed from simulations by averaging the displacement $\|r_{20}(0) - r_{20}(t)\|^2$ of monomer r_{20} of a polymer for time t between $t = 0$ s to 360 s over 200 simulations. The optimal fit of At^α (orange) to the MSD curve from time 1 s to 100 s (dashed vertical lines), corresponds to the polymer's relaxation times, for which we obtained $A = 0.045$, $\alpha = 0.43$. In the inset we plotted the MSD (blue) and model fit (orange) on a log-log scale.

would recapitulate these behaviors by considering independent physical sources of motion such as local interactions, drift, and more.

The Effective Spring Coefficient K_c

What restricts the motion of chromatin loci? As described in the introduction, a number of chromatin tethers exist in the nucleus, such as the centromere and telomeres in budding yeast. The force of these and other tethers cannot easily be measured *in vivo* but they can be inferred from SPTs by estimating an **effective spring coefficient K_c** [4,33,61]. A trajectory could be

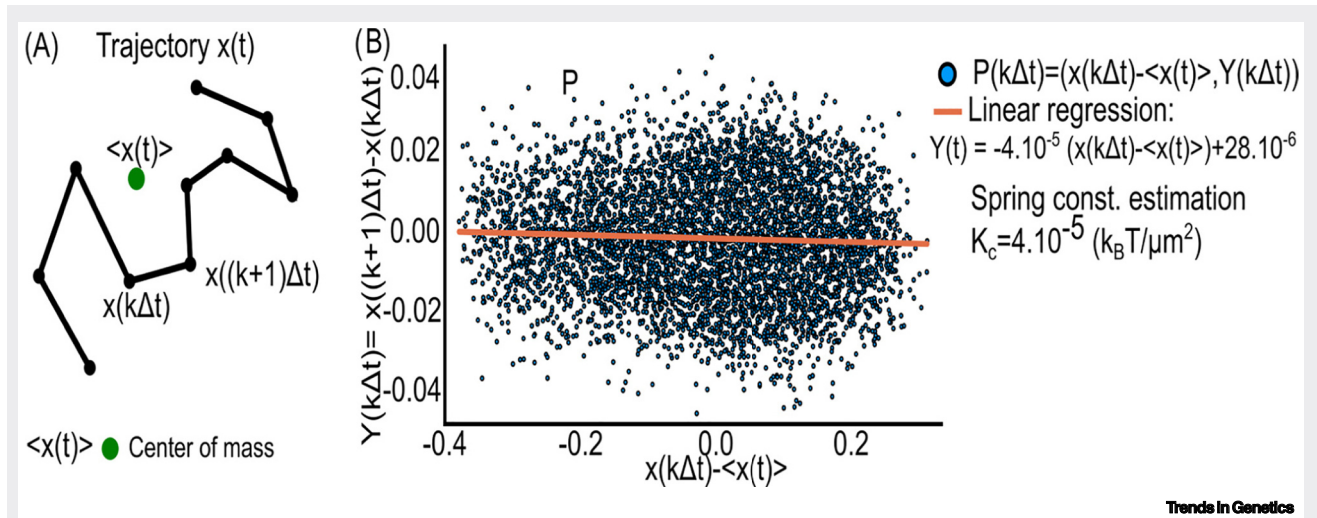


Figure II. Computing the Spring Constant from a Locus Trajectory. (A) Trajectory $x(t)$ of a tagged locus of the chromatin is sampled at discrete time $k\Delta t$ ($k = 0, 1, \dots, N$), where the center of mass $\langle x(t) \rangle$ (green) is computed over time. (B) To estimate the tethering force k_c (spring constant) acting on a locus, we use Equation 1 for either an experimental or simulated trajectory. To avoid numerical instabilities, the constant k_c is estimated using linear regression (orange line) of points $P(k\Delta t) = (x(k\Delta t) - \langle x(t) \rangle, Y(k\Delta t))$, (blue) with $Y(k\Delta t) = x((k + 1)\Delta t) - x(k\Delta t)$. The spring constant k_c is the coefficient of $x(k\Delta t) - \langle x(t) \rangle$. Here we obtained $k_c = 4 \times 10^{-5} k_B T / \mu m^2$.

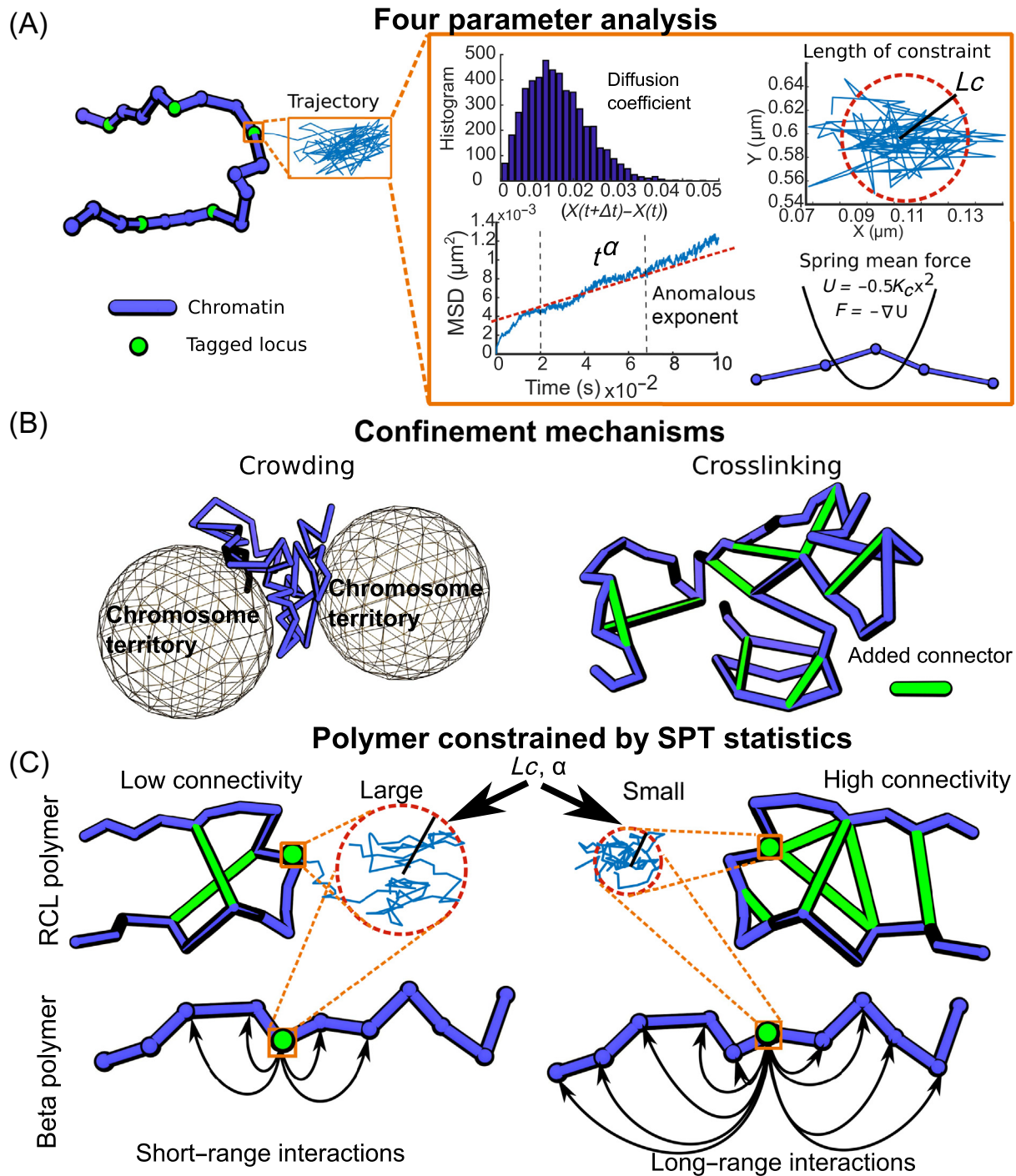
confined either by obstacles or by a field of force. How can we differentiate between these two possibilities? This question can be addressed by using a polymer model, where a tethering force is generated by a potential well $U_{\text{ext}}(\mathbf{R}_n) = \frac{1}{2} K_c (\boldsymbol{\mu} - \mathbf{R}_n)^2$ centered at a point $\boldsymbol{\mu}$ and applied at a monomer R_n . The spring constant K_c has to be estimated from data (Figure 1A, Key Figure and Box 2). The field of force U_{ext} should influence the motion of any locus and thus could be extracted from trajectories. This tethering not only affects the motion of the whole polymer (chromosome) but can arise from interactions of the locus with other chromosomes or nuclear substructures such as the nuclear envelope. A procedure has been developed for freely moving particles [54], requiring many redundant trajectories exploring the same microenvironment. However, for a single-long trajectory that does not come back too many times on itself, there may not be necessarily enough data points. To overcome this difficulty, a recent method [61] considers consecutive displacements $R_c(t + \Delta t) - R_c(t)$ as independent when a trajectory is recurrent, returning back on itself many times. In this case, it is possible to estimate the spring constant K_c , as described in Box 2 and [61]. To conclude, when a trajectory folds back on itself many times, it is possible to extract a field of force [62].

As described in the introduction, artificial removal of cohesin in S phase cells increases chromatin motion. Interestingly, removal of cohesin in G1 phase cells, where the sister chromosome is absent, also marginally increases chromatin motion. This suggests a role for cohesin as a possible connector or tether in budding yeast [27,33]. Removal of such a tether (cohesin) decreases K_c [33].

For motion confined due to crowding only, applying the above procedure to a Brownian particle would not lead to the estimation of any forces (which means $K_c = 0$ [61]), because there is no field of force, except for the points in very close vicinity of the large obstacles [53] that restrict motion (Figure 1B). For a monomer located on a polymer, we expect $K_c \neq 0$ to reflect the external forces acting on the chain. Hence, estimating K_c for a locus near obstacles such as the nucleolus or the

Key Figure

From Single-Particle Trajectory (SPT) of Chromatin Locus to Polymer Models



Trends in Genetics

(See figure legend at the bottom of the next page.)

boundary of the nucleus would result in a non-zero force estimate ($K_c > 0$). When obstacles are completely intermingled, these estimations are less robust.

Effective Diffusion Coefficient D_c

Accurately estimating the diffusion coefficient from an SPT is not an easy task and much work has been done to develop estimators to do so [63]. Much like the anomalous exponent, D_c relies on a suitable number of points. A study measuring the diffusion of fluorescent beads in a glycerol solution generated extremely long trajectories [64] that could be decomposed into short trajectories of variable length and enabled measurement of the relative error of the diffusion coefficient. Segments consisting of 100 time points had a relative error of 25% and increasing the number of time points to 1000 decreased the error to 10%. Most chromatin loci tracking experiments record 200 time points. Therefore, it is unsurprising that the same loci in different cells can have very different diffusion coefficients, demonstrating the heterogeneity of this parameter. Others have tried to make sense of the diffusion coefficient by segmenting trajectories at points where D_c changes [65].

Since the diffusion coefficient D_c is highly variable between different cells, estimating it from multiple trajectories will give far greater statistical power than from a single one. Indeed, computing the diffusion coefficient of a massive number (10^4 – 10^5) of super-resolution trajectories allows for the reconstruction of a diffusion map inside the cell. This can be used for a variety of cellular fluorescently tagged proteins in different cellular compartments, including histones and receptor proteins [47,53-55,66-73].

To conclude, the four parameters described above (L_c, α, K_c, D_c) can be estimated from trajectories and they provide complementary information about the statistical properties of chromatin loci [3,4]. In addition, their estimation does not assume or require any underlying physical structure such as a polymer model, which will come in a second stage for the interpretation and the reconstruction of the underlying chromatin organization at a given spatial and temporal scale (Box 1).

Constructing Polymer Models that Represent Chromatin Dynamics and Structure

How is a polymer model selected from the statistics of SPTs? For the **Rouse polymer model**, consisting of monomers connected by springs, the anomalous exponent of a monomer whose position in time is $X(t)$ is $\alpha = 0.5$ ($\langle |X(t + \Delta t) - X(t)|^2 \rangle \sim t^{0.5}$). This is true at a time shorter than the slowest relaxation time of the polymer. This statistical property deviates from Brownian motion where $\alpha = 1$. This difference in the exponent α exemplifies the polymer nature of single locus dynamics. Recently, new classes of polymer models were introduced where mid- and long-range forces are added between all monomers. These long-range forces result in the additional coupling between monomers reviewed in [9]. The strength of the long-range forces coupling can be tuned to modify the anomalous exponent of a monomer in the range of $\alpha \in (0 - 0.5)$ such that the anomalous exponent can be prescribed [13]. Stronger coupling leads to a lower anomalous exponent, while the limit of weak coupling between distant monomers is the limit of the linear chain, the Rouse model ($\alpha = 0.5$) [13].

Figure 1. (A) Extraction of four parameters from a trajectory of a single locus (green). The four parameters extracted are: the diffusion coefficient D_c , the length of constraint L_c , the anomalous exponent α , and the spring constant K_c of a parabolic potential well (red box). (B) Two possible confinement mechanisms: crowding can be generated from the exclusion of a polymer from chromosome territories, thus leading to the restriction of a locus (left), or confinement can be induced by added crosslinkers (such as CTCF, cohesin, condensin) to the chromatin fiber. (C) Construction of polymer models constrained by SPT statistics: values of parameters such as L_c or α can be used to constrain polymer such as the randomly crosslinked (RCL) polymer (top) or the beta polymer (bottom). For example, L_c and α small can be recovered by adding the right number of connectors (green) or long-range interactions (arrows) to RCL and beta polymer model, respectively. Abbreviation: MSD, mean-squared displacement.

Following DSB induction, the overall dynamics of a broken chromatin locus increased. The anomalous exponent of a locus on the DNA increased from 0.38 (before break) to 0.53 (after break induction) [4]. A similar effect was observed in that study for the *MAT* locus. Reconstructing chromatin when the motion of loci is characterized by $\alpha > 0.5$ is more complicated, as different types of forces are possible: combining a **β -polymer model** with a deterministic drift [4] increases the anomalous exponents. Oscillatory motion of the whole nucleus can also lead to such an increase in α [4]. At this stage, polymer models and numerical simulations have revealed an expansion of chromatin at the site of a DSB, a prediction that was confirmed by super-resolution microscopy [4]. An increase in α and a reduction of K_c (Box 2), was associated with an increased motion of the adjacent loci [3,4]. This reduction could be due to reduced tethering. Supporting this hypothesis, chromatin decompacts at the site of a DSB, likely due to the loss of histone proteins. Loss of histones may reduce the ability of the locus to interact with other chromatin loci or nuclear components. To conclude, polymer models can drive a testable hypothesis and can lead to the design of experiments to confirm the theoretical predictions.

We would like to mention an alternative approach to use a polymer model to reconstruct chromatin dynamics. It consists of using a kernel representation of anomalous diffusion, suggesting that a change in α is associated with the visco-elastic nucleoplasm, which would result in additional correlations acting on chromatin [60,74–76].

Polymer Models with Connectors Reflect *In Vivo* Chromatin Dynamics

There are different ways to study the effect of dynamics coming from interactions between distant chromatin sites. One way is to use a model where the monomers of a polymer are connected randomly with transient connectors (binder model or random loop model [10,12]) or fixed connectors (**randomly crosslinked (RCL) model** [14,77]) (Figure 1C). The advantage of using connectors to describe chromatin dynamics/interactions is that connectors exist in biology, specifically in the form of **CTCF** and cohesin that mediate chromatin looping [78]. Adding connectors leads to an anomalous exponent < 0.5 . An exact relationship between the number of connectors and the anomalous exponent has not been derived. However, the underlying mechanism is similar to the β -polymer model: the connection between monomers couples their dynamics and reduces α .

Connectors offer an alternative confinement (restriction) mechanism to crowding through crosslinking (Figure 1B). Changing the number and distribution of connectors affect the four parameters described in the section ‘Chromatin Locus Dynamics Revealed by SPTs’ (Figure 1C). For example, a reduction of the length of constraint L_c in parallel with a reduction of the anomalous exponent α and an increase in the local tethering force spring K_c is associated with an increase in the number of connectors and chromatin condensation. However, no changes are expected to be seen in the diffusion coefficient [4]. Conversely, a decrease of the diffusion coefficient is directly connected to an increase of crowding [79] obtained by adding sufficiently large obstacles compared with the size of the observed loci [77].

To conclude, changing the number of connectors between chromatin loci has several consequences: First, only a few connectors are required to see a deviation from Rouse polymer dynamics. Second, connectors can be positioned at random and not at specific locations, leading to a spectrum of anomalous exponents at each locus. The number of connectors can be estimated using the encounter probability of loci coming from existing HiC data [77]. The number of connectors seems to play a key role in defining topologically associating domains (TADs), gene regulation, and organization across cell differentiation [80,77].

Classifying Forces That Constrain Locus Dynamics

What restricts the motion of a chromatin locus? Restriction can result from confinement and/or tethering. In experiments, we usually observe one or two loci simultaneously. Hence, it is not yet possible to reconstruct all independent forces acting on each monomer in the polymer. Attempts to reconstruct tethering forces acting on a locus assume that the restriction could result from a parabolic potential energy acting on an unknown site on the chromosome, as discussed in the section 'The Effective Spring Coefficient K_c ' and [Box 2](#). This classical model is used in the theory of chemical reactions and is characterized by a finite parabolic well, truncated at a specific height [73]. Another possibility, as discussed above, is that to account for motion restriction, random or fixed connectors are added to a Rouse polymer, leading to slower motion (smaller α) of its monomers ([Figure 1B](#)). This modified polymer would lead to an apparent restricted motion. Tethering, associated with external forces acting on a locus, limits the span of space sampled by the locus.

Once an overall force is computed from SPTs, due to the nature of the polymer, an additional step is needed to differentiate the internal (due to chromatin internal properties) from the external forces. This step involves a deconvolution procedure [61]. When the chromatin is approximated as a Rouse polymer model, it is then possible to recover the spring constant K_c of the effective external force from the total force, when we know the genomic distance between the tagged locus and the one that force is applied to ([Box 2](#)). The case of multiple forces was resolved in the supplemental information of [61]. For more elaborate models, numerical simulations are used to recover external forces.

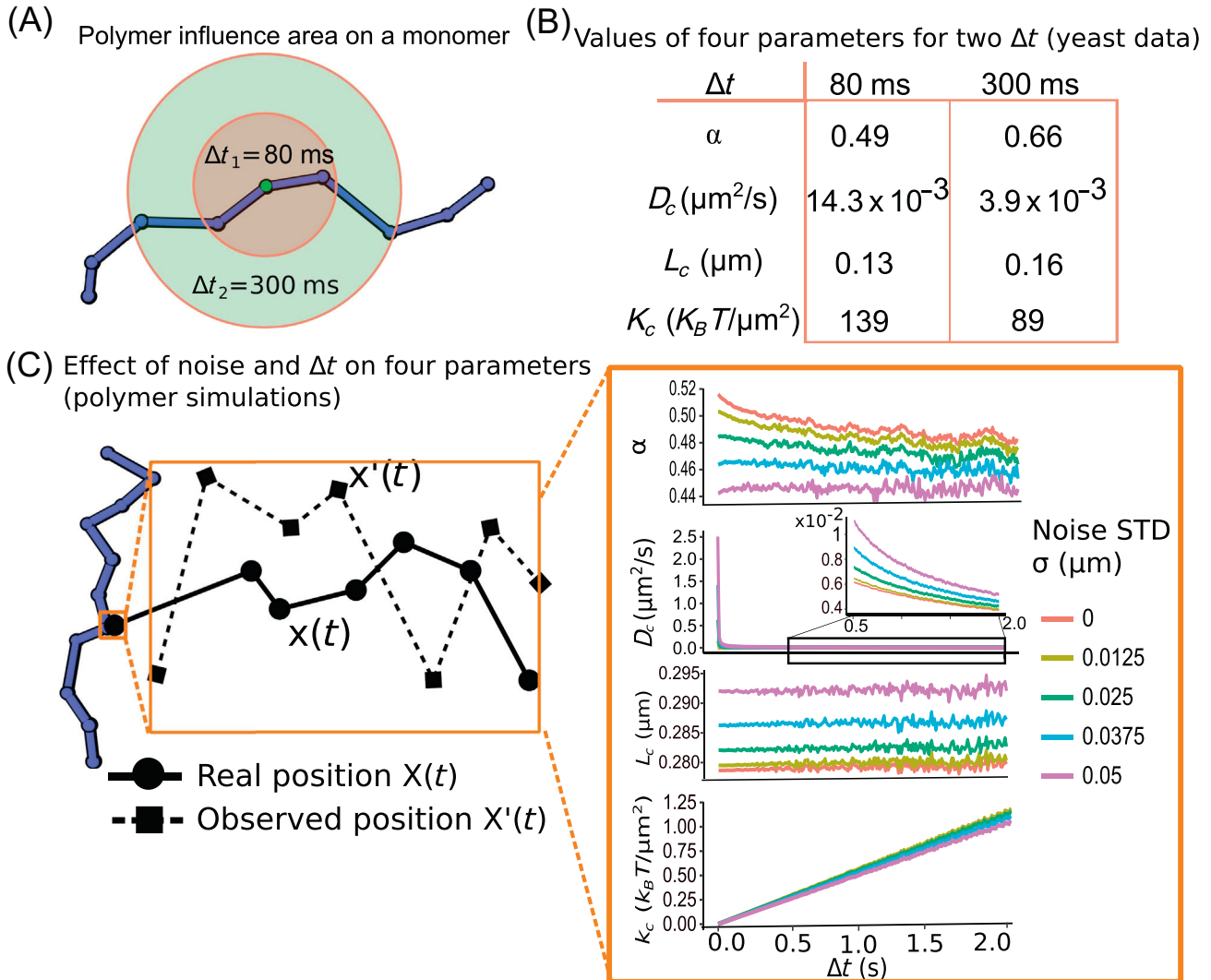
To conclude, the origin of deterministic forces acting on chromatin is still poorly understood, but polymer models suggest that connectors that restrict chromatin loci motion lead to apparent forces. Measuring the correlated motion of multiple loci may be useful to better estimate those forces.

How Does the Sampling Time Step Δt Influence the Four Parameters?

How does the sampling time Δt influence the biophysical parameters extracted from SPTs? The four parameters mentioned above depend on Δt ([Box 2](#)). For example, in yeast, for the *MAT* locus, when $\Delta t = 80$ ms, $\alpha = 0.49$ ([Figure 2B](#)), while for the same locus for $\Delta t = 300$ ms, α increases to 0.66. A similar effect is observed for the other parameters [9]. In principle, if we were to estimate α in a simple polymer (e.g., using Brownian motion or the Rouse model), it would have been independent of Δt [81]. Indeed, at intermediate times, the dynamics of a monomer obeys a power-law and thus is independent of the timescale. So why do we see a difference when observing chromatin at different timescales?

Chromatin, like other polymers, has multiple relaxation times. The shorter relaxation times are associated with smaller genomic lengths and larger times are associated with larger lengths ([Figure 2A](#)). By choosing a specific time step, we establish a cutoff below which locus dynamics are no longer observed. For example, if we take $\Delta t = 80$ ms, all faster processes occurring on chromatin are averaged when estimating the parameters. Imagine a fly in a room. If we observe it every 2 hours, it will have had enough time to explore the whole room (sample all positions), meaning that we will observe the fly in its favorite positions (equilibrium distribution) but cannot learn anything about its dynamics. However, if we observe the fly every second, we capture its trajectory from one place to the next, allowing us to extract dynamical parameters such as its velocity. Applying the same concept to measuring chromatin dynamics, it is important to choose a timescale that is relevant to the dynamics we wish to measure.

Thus, the choice of Δt is critical; it should not be too small (that would only capture the motion of a single monomer) or too large (when the entire polymer can move by diffusion in a confined



Trends in Genetics

Figure 2. Influence of the Sampling Rate Δt and Localization Noise on Single-Particle Trajectory (SPT) Statistics. (A) The region of influence on a locus (green) depends on the sampling rate Δt : as Δt increases the fraction of the polymer influencing the motion of a single locus increases, at 80 ms (brown) the region is smaller than the one obtained at 300 ms (green). (B) Example of changes in the four parameters with respect to the sampling rate Δt , obtained from yeast SPTs [4]. (C) Influence of the localization noise on SPTs. The localization noise generates a Gaussian error on the position of loci at each time step Δt . Note, this noise can affect the four parameters: the anomalous exponent α , diffusion coefficient D_c , length of constraint L_c , and the spring constant K_c .

environment), but should be chosen in an intermediate time regime, as predicted from the anomalous behavior of a monomer [4,13]. We note that a timescale analysis, changing Δt from 10 ms, 100 ms to seconds has recently revealed much less impact of chromatin on single locus dynamics, with an anomalous exponent around 0.5 [82]. This is in contrast with an early study [59] of telomere dynamics in mammalian cells, where α changed from 0.32, when estimated in the range of $[10^{-2}; 1]$ s, to 0.51 in $[1; 100]$ s.

When looking at chromatin at $\Delta t = 300$ ms, the larger value of α suggests that this scale is compromised by additional factors such as nuclear rotation. Another effect of Δt concerns the interpretation for the tracking localization noise (Figure 2C), where a Gaussian error of amplitude

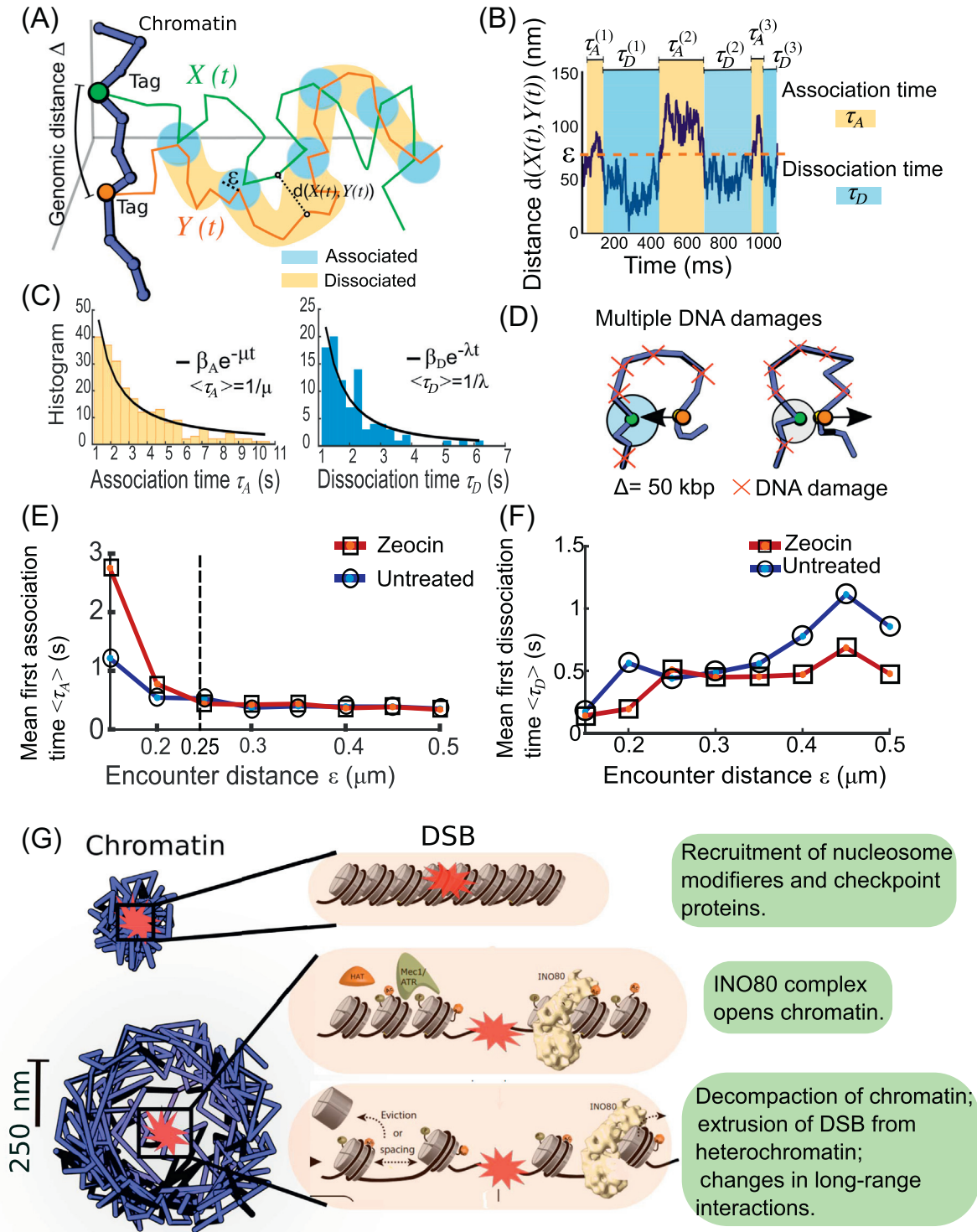
σ is added to the real position X , so that the measured position is $X' = X + \sigma\xi$. Such localization error affects the value of the measured (effective) diffusion coefficient compared with the real diffusion coefficient D_{real} , leading to a shift $D_{measured} = D_{real} + \frac{\sigma^2}{2\Delta t} + A\sigma^2 \text{div}f$, where A is a constant and f is the force applied to the tagged loci [83]. Increasing the localization error changes the estimation of all parameters. The effect of Δt , through the localization error, influences α , D_c , and k_c (Figure 2C). The diffusion coefficient can also depend on Δt (Figure 2B). In a region with well-spread obstacles, small Δt captures motion in the space between obstacles. However, increasing Δt means looking at chromatin at larger steps each frame, which would result in it bumping into obstacles and a reduced diffusion coefficient. An analysis of the effect of obstacle density on the diffusion coefficient of a Brownian particle can be found in [79].

In summary, the choice of Δt affects both the localization error and the biological processes we can follow. Ideally, localization error of the microscope will be known for the Δt chosen. As a general guideline, if the process we wish to follow occurs on chromatin, Δt must be small enough such that nuclear drift, or other motion artifacts, do not affect the measurements. It is worthwhile noting that if one is looking for a biological effect on chromatin mobility it may be beneficial to look for it at multiple timescales. Future investigations are needed to clarify what exactly can be revealed from the chromatin at small and large Δt and how to reconcile the different values of parameters computed for different Δt .

Statistic of Two Simultaneous Tracked Loci Reveals Chromatin Dynamics at the 250 nm scale

Are there new features or biophysical information contained in trajectories of two loci tracked simultaneously that are not contained in loci tracked individually? A number of studies have tracked two loci to extract additional information about chromatin dynamics and interactions [3,75,84,85]. Using the four biophysical parameters mentioned above, each locus could be analyzed separately. However, there are a number of biological processes that could be better understood by studying the interaction of two genomic loci simultaneously (Figure 3A). For instance, chromatin looping in the context of enhancer/promoter contacts and repair of DNA DSBs by HR. Such processes have an associated encounter (looping) time τ_E . Once the two loci meet, they will stay together until drifting apart and this process has a dissociation time, τ_D , which is related to the binding energy between them (Figure 3B,C). The statistics of these two times seems to obey a Poissonian distribution (Figure 3C). We recall that the Poissonian decay of the encounter time distribution τ_E was predicted by the polymer looping theory [9,84,86,87] because it is a rare event.

The method of analysis is divided into several steps: first, two-locus trajectories $X(t)$ and $Y(t)$ are collected (Figure 3A). Then an arbitrary threshold length ($T = \varepsilon$) that defines an encounter distance is chosen, which we can vary between tens and hundreds of nanometers. In the second step, the distance $d(t) = |X(t) - Y(t)|$ is computed from trajectories. The third consists of a segmentation, where the time intervals before the two-locus encounter for the first time, defined by $d(t) > \varepsilon$, are collected. It leads to the time series $[\tau_{E1}, \dots, \tau_{En}]$ (Figure 3B, yellow band). Then a second time series for the distribution of times before the two loci dissociate $[\tau_{D1}, \dots, \tau_{Dm}]$ (Figure 3B, blue band) is also collected. The last step of analysis consists of plotting the distribution of time. Interestingly, the two time distributions τ_E and τ_D can be well fitted by exponentials (continuous black lines in Figure 3C). This procedure confirms the Poissonian distribution (noncorrelated events) of the distribution. This Poissonian property is valid for several genomic distances Δ between the two loci [84]. However, the mechanism of two loci dissociation is not that clear: if a physical mechanism prevents the two loci from separating, then the dissociation time distribution can also be



Trends in Genetics

(See figure legend at the bottom of the next page.)

approximated by a single exponential distribution, similar to two molecules that dissociate. Two-locus dynamics were collected for five genomic distances Δ in the range [23.5, 100.8] kbps [85], by tracking trajectories at a time interval of 300 ms over 60 s. The **passage time analysis** [84] revealed that the mean encounter time $\langle \tau_E \rangle$ decreases in the range $\epsilon \in [0, 0.25]$ μm , but was independent of the encounter distance for $\epsilon > 0.25$ μm . In comparison, the mean dissociation time $\langle \tau_D \rangle$ increases with ϵ in the range [0, 0.5] μm . The passage time analysis was also applied before and after the use of the drug **Zeocin** 500 $\mu\text{g}/\text{ml}$, which induces DNA damages at random positions of the chromatin (Figure 3D, top, red crosses): two loci located at a distance $\Delta = 50$ kbp apart, tracked over 60–120 s at 300 ms rate [3], have a mean duration $\langle \tau_E \rangle$ that decreases with respect to the distance threshold ϵ , both in the untreated and Zeocin treated cases (Figure 3D). A plateau is reached in 500 ms for $\epsilon = 0.25$ μm , showing that the encounter time does not depend on ϵ above 0.25 μm . Interestingly, the mean encounter time $\langle \tau_E \rangle$ (Figure 3E) is slower following induction of a DSB, while the mean dissociation time $\langle \tau_D \rangle$ is faster (Figure 3F). Thus, panels E–F of Figure 3 reveal that changes in chromatin organization are possible below 250 nm following DSB. In addition, the changes in $\langle \tau_E \rangle$ and $\langle \tau_D \rangle$ can be due to a local decompensation of chromatin below 250 nm, so that it takes less time for two loci to dissociate after DSB, while it takes more time to meet. This result suggested that chromatin is decondensed and probably less crowded at the spatial scale of the order of the distance Δ between the two loci, while it is more crowded far away. This crowding may be due to a local depletion of material locally after DSB, which is relocated further away from the break site. To conclude, distributed DSBs impair recurrent chromatin motions only at a scale below 0.25 μm , suggesting that this spatial scale characterizes the local chromatin organization in which undamaged loci can freely move, but become restricted above it (Figure 3G). Possibly future recordings of multiple loci at the same time could reveal higher-order chromatin organization and could be used to determine the minimum number of crosslinkers compatible with the statistics of the recurrent loci behavior.

Local Chromatin Environment Revealed by Coarse-Grained Polymer Models

Understanding how chromatin moves in a confined environment remains a challenge. What could be the mechanism that confines chromatin? A modeling approach can be used to address this question by transforming the information contained in the four parameters mentioned in the section ‘Chromatin Locus Dynamics Revealed by SPTs’ into crosslinkers to be added on polymer models.

Crosslinkers Constrain Chromatin Motion

We recall that short- and long-range interactions of crosslinkers can constrain chromatin motion. Indeed, there are $\sim 100\,000$ CTCF binding sites identified in the human genome [88,89], but not all binding sites are occupied at any moment of time. Genomic loops mediated by structural proteins vary in the range of 15–123 kbp in HeLa cells, with a mean of 86 kbp [90]. A significantly larger cohesin loop of ~ 370 kbp was measured in [91]. Bound cohesin is not distributed uniformly along the chromosome, having a higher concentration near centromeres and overall average

Figure 3. Multiple Loci Single-Particle Trajectory (SPT) Statistics. (A) Two loci (green, orange), separated by a genomic distance Δ , generate two trajectories $X(t), Y(t)$, showing regions where they are located inside balls of radius ϵ (blue) separated by regions (yellow) where the trajectories are far apart. (B) Distance $D(X(t), Y(t))$ versus time. When $D(X(t), Y(t))$ is lower than a threshold ϵ , trajectories are classified as associated (A, blue) and characterized by the time (dissociation time τ_D) it takes for the two trajectories to separate. Conversely, when $D(X(t), Y(t)) > \epsilon$, trajectories are dissociated (A, yellow), and characterized by the time (association time τ_A) it takes for the two trajectories to enter for the first time into a region of radius $\leq \epsilon$. (C) Distribution of association and dissociation time, characterized by a single exponential. (D) Schematic representation of two loci association (left) and dissociation (right) dynamics with multiple DNA damages (red crosses). (E) Mean first association time $\langle \tau_A \rangle$ versus the encounter distance ϵ for Zeocin (red squares) and untreated (blue circles) chromatin. (F) Mean first dissociation time $\langle \tau_D \rangle$ versus the encounter distance ϵ for Zeocin (red squares) and untreated (blue circles) chromatin. (G) Consequences of DNA damages of local chromatin reorganization. Material is extruded following double-strand break (DSB).

spacing of 10 kb apart [92], see also [93–95]). In addition, cohesin binding sites correlate with the position of DNA replication origins [96]. Although CTCFs, cohesin, and condensin molecules are bound to chromatin, it is still unclear how exactly they participate in loop formation. But CTCF residence time is ~ 1 min in mouse embryonic stem cells [97]. Approximately 80% of CTCF molecules bind transiently and nonspecifically to the chromatin, with a residence time of ~ 0.2 – 0.6 s [98], whereas the residence time for a residual fraction of CTCF is in a wide range between ~ 4 s and >15 min. Residence times for cohesin are longer than those of CTCF and are cell cycle dependent. In G1, $\sim 30\%$ of cohesin is bound to chromatin with a residence of ~ 6 h, whereas in G2 $\sim 45\%$ of cohesin is bound with a residence time of ~ 24 min, as measured in [78]. Similar times of ~ 20 min were also measured in [97].

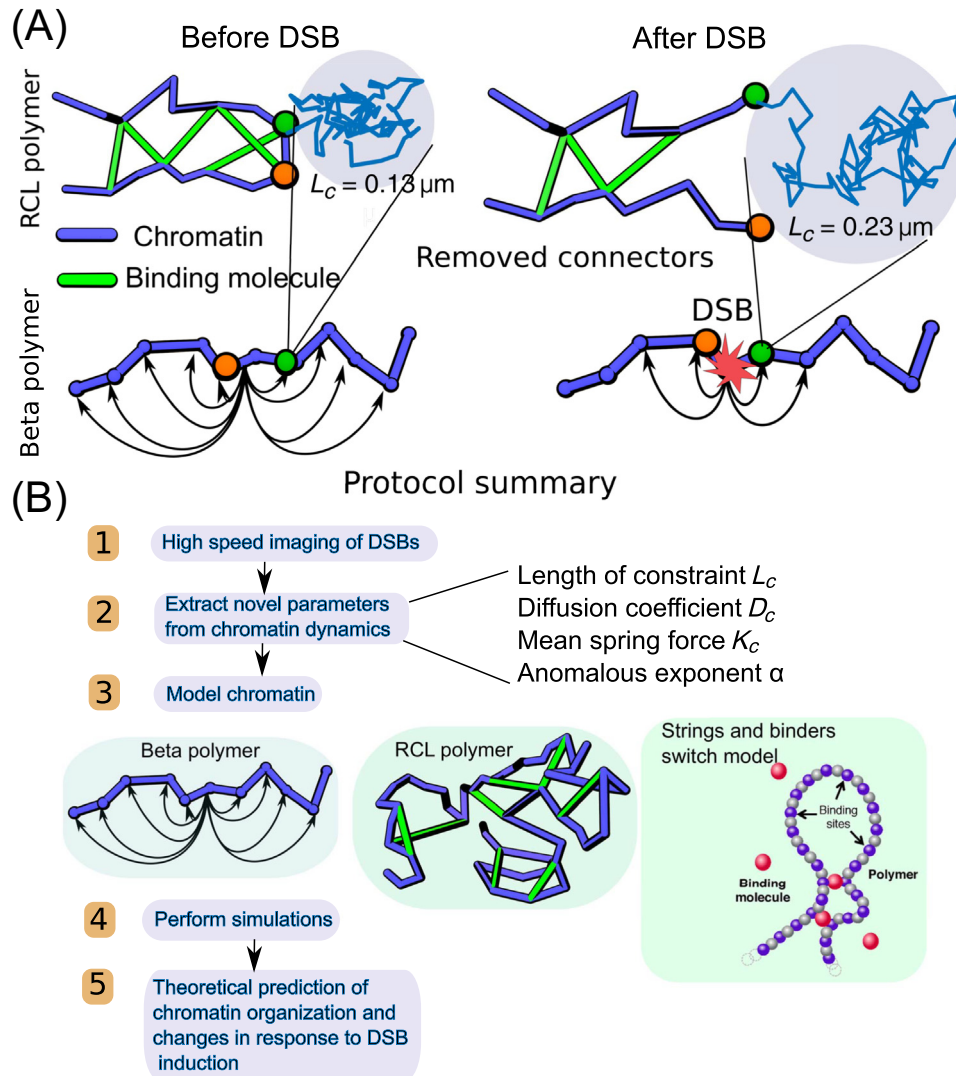
In that context, two types of polymer models have been used to account for these binding molecules: those with transient [10,12] and those with permanent but randomly positioned connectors [14,77]. The local chromatin environment, including constraints, can be simulated using polymer models such as the β -polymer or RCL model [14,77]. The later model describes chromatin containing crosslinkers, positioned at random places. We recall that the RCL polymer is composed of a linear Rouse backbone of N monomers, connected sequentially by harmonic springs. In each realization of the polymer, N_c spring connectors are added (Figure 4A) between randomly chosen non-nearest monomers pairs. This parsimonious addition of connectors accounts for binding molecules such as CTCF and cohesin or condensin, and their semi-random position can generate the heterogeneity in chromatin architecture observed across a cell population.

To conclude, the key parameter that reflects the constraint of the chromatin encounter probability is the number of connectors in a defined subchromatin region, but not necessarily their position, as long as they are uniformly distributed. Transient and static connectors lead to similar statistical properties over a timescale longer than the transient detachment and reattachment of each connector.

How Many Crosslinkers Are Needed to Agree with a Small Length of Constraint?

CTCF, cohesin, and condensin contribute to chromatin organization, and crosslinker proteins play an important role in maintaining the structure of the nucleolus [99]. Condensin and High Mobility Group protein 1 (Hmo1) could form dynamic crosslinks that phase-separate the nucleolus from the rest of chromatin, ensuring that rDNA loci stay within a single nuclear subdomain. As a consequence of these heterogeneous phases, chromatin motion is restricted and could be described by adding connectors to a polymer model. In that case, how many connectors should be added and where? In a recent method [77] using **HiC data**, the encounter probability was used to find short-range (intra-TAD organization) and long-range connectors. The simulated encounter probability map, which appears to be very similar to the empirical HiC one, suggested that the reconstructed polymer model is an adequate representation of chromatin at the scale of the HiC data. Once such a polymer is constructed, it is then possible to explore transient properties such as the time and the probability for two loci to meet before meeting the third one. Thus, this analysis reveals the local chromatin properties.

Another possible calibration of crosslinkers is obtained by using the length of constraint L_c described above: before and after the induction of a DSB, the length L_c increases from 0.13 (before) to 0.23 μm (after) DSB [4]. In that case, the number of needed connectors for a polymer with a total length of $N = 100$ monomers varied from $N_c = 130$ to 125 , respectively (Figure 4A) [84]. Interestingly, if a large number of crosslinkers is required to condense a polymer to a small blob, surprisingly, only $\sim 4\%$ are removed to create the decondensed DSB phase. In addition, the



Trends in Genetics

Figure 4. Chromatin Modification Represented by Polymer Models Before and After Double-Strand Break (DSB). (A) An increase of L_c following DSB can be obtained by removing connectors (green) in randomly crosslinked (RCL) polymer model (top) or by removing long-range forces in the beta polymer model (bottom). (B) Summary of the general procedure of converting information contained in the four parameters extracted from single-particle trajectory of chromatin loci into a polymer representation. This polymer can be used to generate statistics not contained in the original trajectories.

mean radius of gyration ($\langle R_g \rangle \approx 150 \text{ nm}$) is mostly unchanged between the unbroken locus and DSB. By removing the number of connectors, the mean maximal distance between the two monomers increases from $0.33 \mu\text{m}$ in the unbroken case to $0.75 \mu\text{m}$ after DSB. Separation of the two DSB ends cannot be too large due to remaining connectors that maintain the two extremities. To conclude, randomly positioned crosslinkers can be used to model chromatin condensation and dynamics. Their minimum number can be adjusted to match experimental data of SPTs and HiC, offering a simple tool to represent chromatin organization at a given spatial scale, that can be used to explore the local chromatin environment and dynamical properties.

Concluding Remarks

As the world of chromatin molecular biology and biophysics become more entangled, it is essential to build a set of reliable tools to easily analyze biological data. Here, we have described techniques and tools to study SPT data as well as how to use polymer models to interpret these results in the context of chromatin suborganization (see Outstanding Questions). We further presented how to extract information from correlated loci analysis and how to interpret the changes in parameter values when the sampling rate Δt is changing.

Models are a step towards a unified tool of SPT data, with data generated by chromatin conformation capture techniques such as HiC (Figure 4B). Such a tool would be immensely useful as it would take into account the physical dynamics of chromatin at a local level, while also giving an overview of interactions throughout globally. This type of unified model would allow us to better understand a number of complicated biological processes, such as enhancer/promoter organization during transcriptional reprogramming, homology search during DSB repair, and CRISPR/Cas9 editing. In particular, simulating the effects of integrating viral DNA on the chromatin environment would give new insight into how viruses cause mutations and ultimately disease.

Acknowledgments

This work was supported by the Office of the Provost, Faculty of Arts and Sciences, and Center for Advanced Imaging at Harvard University. Research by D.H. is supported by FMR team (DEQ20160334882) and ANR-18-NEUC-0001.

Supplemental Information

Supplemental information associated with this article can be found online at <https://doi.org/10.1016/j.tig.2019.06.007>.

References

- Strick, T. *et al.* (2000) Twisting and stretching single DNA molecules. *Prog. Biophys. Mol. Biol.* 74, 115–140
- Strick, T. *et al.* (2002) Stretching of macromolecules and proteins. *Rep. Prog. Phys.* 66, 1
- Hauer, M.H. *et al.* (2017) Histone degradation in response to DNA damage enhances chromatin dynamics and recombination rates. *Nat. Struct. Mol. Biol.* 24, 99–107
- Amitai, A. *et al.* (2017) Visualization of chromatin decompaction and break site extrusion as predicted by statistical polymer modeling of single-locus trajectories. *Cell Rep.* 18, 1200–1214
- Tiana, G. and Giorgetti, L. (2018) Integrating experiment, theory and simulation to determine the structure and dynamics of mammalian chromosomes. *Curr. Opin. Struct. Biol.* 49, 11–17
- Parmar, J.J. *et al.* (2019) How the genome folds: the biophysics of four-dimensional chromatin organization. *Annu. Rev. Biophys.* 48
- Zimmer, C. and Fabre, E. (2019) Chromatin mobility upon DNA damage: state of the art and remaining questions. *Curr. Genet.* 65, 1–9
- Fabre, E. and Zimmer, C. (2018) From dynamic chromatin architecture to DNA damage repair and back. *Nucleus* 9, 161–170
- Amitai, A. and Holcman, D. (2017) Polymer physics of nuclear organization and function. *Phys. Rep.* 678, 1–83
- Bohn, M. *et al.* (2007) Random loop model for long polymers. *Phys. Rev. E* 76, 051805
- Heermann, D.W. (2011) Physical nuclear organization: loops and entropy. *Curr. Opin. Cell Biol.* 23, 332–337
- Barbieri, M. *et al.* (2012) Complexity of chromatin folding is captured by the strings and binders switch model. *Proc. Natl. Acad. Sci.* 109, 16173–16178
- Amitai, A. and Holcman, D. (2013) Polymer model with long-range interactions: analysis and applications to the chromatin structure. *Phys. Rev. E* 88, 052604
- Shukron, O. and Holcman, D. (2017) Statistics of randomly cross-linked polymer models to interpret chromatin conformation capture data. *Phys. Rev. E* 96, 012503
- Chen, B. *et al.* (2016) Imaging specific genomic DNA in living cells. *Annu. Rev. Biophys.* 45, 1–23
- Seeber, A. *et al.* (2018) Chromosome dynamics in response to DNA damage. *Annu. Rev. Genet.* 52, 295–319
- Smith, M.J. and Rothstein, R. (2017) Poetry in motion: increased chromosomal mobility after DNA damage. *DNA Repair* 56, 102–108
- Heun, P. *et al.* (2001) Chromosome dynamics in the yeast interphase nucleus. *Science* 294, 2181–2186
- Gartenberg, M.R. *et al.* (2004) Sir-mediated repression can occur independently of chromosomal and subnuclear contexts. *Cell* 119, 955–967
- Liu, J. *et al.* (2015) Nanoscale histone localization in live cells reveals reduced chromatin mobility in response to DNA damage. *J. Cell. Sci.* 128, 599–604
- Joyner, R.P. *et al.* (2016) A glucose-starvation response regulates the diffusion of macromolecules. *eLife* 5, e09376
- Levi, V. and Gratton, E. (2008) Chromatin dynamics during interphase explored by single-particle tracking. *Chromosom. Res.* 16, 439
- Weber, S.C. *et al.* (2012) Nonthermal ATP-dependent fluctuations contribute to the in vivo motion of chromosomal loci. *Proc. Natl. Acad. Sci.* 109, 7338–7343
- Nozaki, T. *et al.* (2017) Dynamic organization of chromatin domains revealed by super-resolution live-cell imaging. *Mol. Cell* 67, 282–293
- Krawczyk, P. *et al.* (2012) Chromatin mobility is increased at sites of DNA double-strand breaks. *J. Cell. Sci.* 125, 2127–2133
- Pliss, A. *et al.* (2009) Chromatin dynamics is correlated with replication timing. *Chromosoma* 118, 459–470
- Dion, V. *et al.* (2013) Cohesin and the nucleolus constrain the mobility of spontaneous repair foci. *EMBO Rep.* 14, 984
- Taddei, A. and Gasser, S.M. (2012) Structure and function in the budding yeast nucleus. *Genetics* 192, 107–129
- Jin, Q.-W. *et al.* (2000) Centromere clustering is a major determinant of yeast interphase nuclear organization. *J. Cell. Sci.* 113, 1903–1912

Outstanding Questions

While more and more data have been collected on chromatin dynamics in various organisms and for many different genomic loci, it has yet to be directly shown how changes in chromatin dynamics benefits a biological process. Specifically, how does chromatin movement influence DNA repair?

What is the relationship between chromatin structure and its dynamics? While we know that in yeast, removal of nucleosomes from DNA is correlated with increased loci mobility, little is known in higher eukaryotes.

Which universal polymer model should be used to explain the dynamics of chromatin and its structure in living cells? Additional data on both the movement of chromatin and its structure changes during that movement will probably be required to refine such a model. This will likely come from developments in live-cell microscopy of multiple chromatin loci.

Single-particle trajectories of a chromatin locus reveal the local chromatin dynamics. What else can be revealed by the correlated motion of many loci tracked simultaneously?

In the multiscale chromatin organization, the spatial scale of 200–300 nm seems to correspond to the control of short- and long-range loops. What is the relation between this spatial scale, chromatin regulation, and gene expression?

How can we combine statistics of population and single cell HiC? How does the distribution of the encounter probability extracted from HiC compare with SPTs (which provide statistics of local time dynamics)?

Polymer models have been used to represent DNA reorganization following DSB. How can we converge to a unified polymer model? Shall we keep models as simple as possible, adjusting them for each situation?

30. Hediger, F. *et al.* (2002) Live imaging of telomeres: yKu and Sir proteins define redundant telomere-anchoring pathways in yeast. *Curr. Biol.* 12, 2076–2089
31. Spichal, M. *et al.* (2016) Evidence for a dual role of actin in regulating chromosome organization and dynamics in yeast. *J. Cell. Sci.* 129, 681–692
32. Streckler, J. *et al.* (2016) DNA damage signalling targets the kinetochore to promote chromatin mobility. *Nat. Cell Biol.* 18, 281
33. Verdaasdonk, J.S. *et al.* (2013) Centromere tethering confines chromosome domains. *Mol. Cell* 52, 819–831
34. Bronshtein, I. *et al.* (2015) Loss of lamin A function increases chromatin dynamics in the nuclear interior. *Nat. Commun.* 6, 8044
35. Neumann, F.R. *et al.* (2012) Targeted INO80 enhances subnuclear chromatin movement and ectopic homologous recombination. *Genes Dev.* 26, 369–383
36. Chuang, C.-H. *et al.* (2006) Long-range directional movement of an interphase chromosome site. *Curr. Biol.* 16, 825–831
37. Chen, H. *et al.* (2018) Dynamic interplay between enhancer-promoter topology and gene activity. *Nat. Genet.* 50, 1296
38. Ochiai, H. *et al.* (2015) Simultaneous live imaging of the transcription and nuclear position of specific genes. *Nucleic Acids Res.* 43, e127
39. Germier, T. *et al.* (2017) Real-time imaging of a single gene reveals transcription-initiated local confinement. *Biophys. J.* 113, 1389–1394
40. Nagashima, R. *et al.* (2019) Single nucleosome imaging reveals loose genome chromatin networks via active RNA polymerase II. *J. Cell. Biol.* 218, 1511
41. Dion, V. *et al.* (2012) Increased mobility of double-strand breaks requires Mec1, Rad9 and the homologous recombination machinery. *Nat. Cell Biol.* 14, 502–509
42. Seeber, A. *et al.* (2013) Checkpoint kinases and the INO80 nucleosome remodeling complex enhance global chromatin mobility in response to DNA damage. *Genes Dev.* 27, 1999–2008
43. Cardì, C.P. *et al.* (2018) Nuclear F-actin and myosins drive relocalization of heterochromatic breaks. *Nature* 559, 54
44. Burov, S. *et al.* (2013) Distribution of directional change as a signature of complex dynamics. *Proc. Natl. Acad. Sci.* 110, 19689–19694
45. Tiana, G. *et al.* (2016) Structural fluctuations of the chromatin fiber within topologically associating domains. *Biophys. J.* 110, 1234–1245
46. Maass, P.G. *et al.* (2018) *Spatiotemporal allele organization by allele-specific CRISPR live-cell imaging (SNP-CLING)*, Nature Publishing Group
47. Shaban, H.A. *et al.* Nanoscale mapping of DNA dynamics in live human cells. *bioRxiv* Published online January 5, 2019. <https://doi.org/10.1101/405969>
48. Calderon, C.P. *et al.* (2013) Quantifying transient 3D dynamical phenomena of single mRNA particles in live yeast cell measurements. *J. Phys. Chem. B* 117, 15701–15713
49. Calderon, C.P. and Bloom, K. (2015) Inferring latent states and refining force estimates via hierarchical Dirichlet process modeling in single particle tracking experiments. *PLoS one* 10, e0137633
50. Metzler, R. and Klafter, J. (2004) The restaurant at the end of the random walk: recent developments in the description of anomalous transport by fractional dynamics. *J. Phys. A Math. Gen.* 37, R161
51. Kepten, E. *et al.* (2013) Improved estimation of anomalous diffusion exponents in single-particle tracking experiments. *Phys. Rev. E* 87, 052713
52. Kepten, E. *et al.* (2015) Guidelines for the fitting of anomalous diffusion mean square displacement graphs from single particle tracking experiments. *PLoS One* 10, e0117722
53. Hoze, N. *et al.* (2012) Heterogeneity of AMPA receptor trafficking and molecular interactions revealed by superresolution analysis of live cell imaging. *Proc. Natl. Acad. Sci.* 109, 17052–17057
54. Hozé, N. and Holcman, D. (2017) Statistical methods for large ensembles of super-resolution stochastic single particle trajectories in cell biology. *Annu. Rev. Stat. Appl.* 4, 189–223
55. Holcman, D. *et al.* (2018) Single particle trajectories reveal active endoplasmic reticulum luminal flow. *Nat. Cell Biol.* 20, 1118
56. Oshidari, R. *et al.* (2018) Nuclear microtubule filaments mediate non-linear directional motion of chromatin and promote DNA repair. *Nat. Commun.* 9, 2567
57. Cabal, G.G. *et al.* (2006) SAGA interacting factors confine subdiffusion of transcribed genes to the nuclear envelope. *Nature* 441, 770
58. Backlund, M.P. *et al.* (2014) Correlations of three-dimensional motion of chromosomal loci in yeast revealed by the double-helix point spread function microscope. *Mol. Biol. Cell* 25, 3619–3629
59. Bronstein, I. *et al.* (2009) Transient anomalous diffusion of telomeres in the nucleus of mammalian cells. *Phys. Rev. Lett.* 103, 018102
60. Weber, S.C. *et al.* (2010) Bacterial chromosomal loci move subdiffusively through a viscoelastic cytoplasm. *Phys. Rev. Lett.* 104, 238102
61. Amitai, A. *et al.* (2015) Analysis of single locus trajectories for extracting in vivo chromatin tethering interactions. *PLoS Comput. Biol.* 11, e1004433
62. Zidovska, A. *et al.* (2013) Micron-scale coherence in interphase chromatin dynamics. *Proc. Natl. Acad. Sci.* 201220313
63. Vestergaard, C.L. *et al.* (2014) Optimal estimation of diffusion coefficients from single-particle trajectories. *Phys. Rev. E* 89, 022726
64. Ernst, D. and Köhler, J. (2013) Measuring a diffusion coefficient by single-particle tracking: statistical analysis of experimental mean squared displacement curves. *Phys. Chem. Chem. Phys.* 15, 845–849
65. Yin, S. *et al.* (2018) Detection of velocity and diffusion coefficient change points in single-particle trajectories. *Biophys. J.* 115, 217–229
66. Manley, S. *et al.* (2008) High-density mapping of single-molecule trajectories with photoactivated localization microscopy. *Nat. Methods* 5, 155
67. Frost, N.A. *et al.* (2010) Single-molecule discrimination of discrete perisynaptic and distributed sites of actin filament assembly within dendritic spines. *Neuron* 67, 86–99
68. English, B.P. *et al.* (2011) Single-molecule investigations of the stringent response machinery in living bacterial cells. *Proc. Natl. Acad. Sci.* 108, E365–E373
69. Gebhardt, J.C.M. *et al.* (2013) Single-molecule imaging of transcription factor binding to DNA in live mammalian cells. *Nat. Methods* 10, 421
70. Izeddin, I. *et al.* (2014) Single-molecule tracking in live cells reveals distinct target-search strategies of transcription factors in the nucleus. *eLife* 3, e02230
71. Liu, Z. *et al.* (2015) Imaging live-cell dynamics and structure at the single-molecule level. *Mol. Cell* 58, 644–659
72. Hoze, N. and Holcman, D. (2014) Residence times of receptors in dendritic spines analyzed by stochastic simulations in empirical domains. *Biophys. J.* 107, 3008–3017
73. Holcman, D. *et al.* (2015) Analysis and interpretation of superresolution single-particle trajectories. *Biophys. J.* 109, 1761–1771
74. Weber, S.C. *et al.* (2010) Subdiffusive motion of a polymer composed of subdiffusive monomers. *Phys. Rev. E* 82, 011913
75. Lampo, T.J. *et al.* (2016) Physical modeling of dynamic coupling between chromosomal loci. *Biophys. J.* 110, 338–347
76. Lampo, T.J. *et al.* (2017) Cytoplasmic RNA-protein particles exhibit non-Gaussian subdiffusive behavior. *Biophys. J.* 112, 532–542
77. Shukron, O. and Holcman, D. (2017) Transient chromatin properties revealed by polymer models and stochastic simulations constructed from Chromosomal Capture data. *PLoS Comput. Biol.* 13, e1005469
78. Ghirlando, R. and Felsenfeld, G. (2016) CTCF: making the right connections. *Genes Dev.* 30, 881–891
79. Holcman, D. *et al.* (2011) Narrow escape through a funnel and effective diffusion on a crowded membrane. *Phys. Rev. E* 84, 021906
80. Shukron, O. and Holcman, D. (2019) Heterogeneous cross-linked polymers to reconstruct chromatin reorganization during cell differentiation. *Nat. Commun.* 10, 2626

81. Doi, M. and Edwards, S. (1986) *The Theory of Polymer Dynamics* Clarendon, Oxford
82. Miné-Hattab, J. *et al.* (2017) Multi-scale tracking reveals scale-dependent chromatin dynamics after DNA damage. *Mol. Biol. Cell* 28, 3323–3332
83. Hoze, N. and Holcman, D. (2015) Recovering a stochastic process from super-resolution noisy ensembles of single-particle trajectories. *Phys. Rev. E* 92, 052109
84. Shukron, O. *et al.* (2017) Two loci single particle trajectories analysis: constructing a first passage time statistics of local chromatin exploration. *Sci. Rep.* 7, 10346
85. Dickerson, D. *et al.* (2016) High resolution imaging reveals heterogeneity in chromatin states between cells that is not inherited through cell division. *BMC Cell Biol.* 17, 33
86. Pastor, R.W. *et al.* (1996) Diffusion limited first contact of the ends of a polymer: comparison of theory with simulation. *J. Chem. Phys.* 105, 3878–3882
87. Amitai, A. *et al.* (2012) Computation of the mean first-encounter time between the ends of a polymer chain. *Phys. Rev. Lett* 109, 108302
88. Kim, T.H. *et al.* (2007) Analysis of the vertebrate insulator protein CTCF-binding sites in the human genome. *Cell* 128, 1231–1245
89. Rao, S.S. *et al.* (2014) A 3D map of the human genome at kilobase resolution reveals principles of chromatin looping. *Cell* 159, 1665–1680
90. Jackson, D. *et al.* (1990) The size of chromatin loops in HeLa cells. *EMBO J.* 9, 567–571
91. Haarhuis, J.H. *et al.* (2017) The cohesin release factor WAPL restricts chromatin loop extension. *Cell* 169, 693–707
92. Stigler, J. *et al.* (2016) Single-molecule imaging reveals a collapsed conformational state for DNA-bound cohesin. *Cell Rep.* 15, 988–998
93. Blat, Y. and Kleckner, N. (1999) Cohesins bind to preferential sites along yeast chromosome III, with differential regulation along arms versus the centric region. *Cell* 98, 249–259
94. Weber, S.A. *et al.* (2004) The kinetochore is an enhancer of pericentric cohesin binding. *PLoS Biol.* 2, e260
95. Yeh, E. *et al.* (2008) Pericentric chromatin is organized into an intramolecular loop in mitosis. *Curr. Biol.* 18, 81–90
96. Guillou, E. *et al.* (2010) Cohesin organizes chromatin loops at DNA replication factories. *Genes Dev.* 24, 2812–2822
97. Hansen, A.S. *et al.* (2017) CTCF and cohesin regulate chromatin loop stability with distinct dynamics. *eLife* 6, e25776
98. Agarwal, H. *et al.* (2017) Direct observation of cell-cycle-dependent interactions between CTCF and chromatin. *Biophys. J.* 112, 2051–2055
99. Hult, C. *et al.* (2017) Enrichment of dynamic chromosomal crosslinks drive phase separation of the nucleolus. *Nucleic Acids Res.* 45, 11159–11173